



HAL
open science

Mechanically Robust Antibacterial Nanopapers Through Mixed Dimensional Assembly for Anionic Dye Removal

P. Nizam, Vishnu Arumughan, Alosly Baby, M. Sunil, Daniel Pasquini, Ange Nzihou, Sabu Thomas, Deepu Gopakumar

► To cite this version:

P. Nizam, Vishnu Arumughan, Alosly Baby, M. Sunil, Daniel Pasquini, et al.. Mechanically Robust Antibacterial Nanopapers Through Mixed Dimensional Assembly for Anionic Dye Removal. *Journal of Polymers and the Environment*, 2020, 28, pp.1279-1291. 10.1007/s10924-020-01681-3 . hal-02496909

HAL Id: hal-02496909

<https://imt-mines-albi.hal.science/hal-02496909>

Submitted on 17 Jul 2020

HAL is a multi-disciplinary open access archive for the deposit and dissemination of scientific research documents, whether they are published or not. The documents may come from teaching and research institutions in France or abroad, or from public or private research centers.

L'archive ouverte pluridisciplinaire **HAL**, est destinée au dépôt et à la diffusion de documents scientifiques de niveau recherche, publiés ou non, émanant des établissements d'enseignement et de recherche français ou étrangers, des laboratoires publics ou privés.

Mechanically Robust Antibacterial Nanopapers Through Mixed Dimensional Assembly for Anionic Dye Removal

P. A. Nizam¹ · Vishnu Arumughan^{1,2} · Alosy Baby¹ · M. A. Sunil³ · Daniel Pasquini⁴ · Ange Nzihou⁵ · Sabu Thomas¹ · Deepu A. Gopakumar⁵ 

Abstract

There is a piqued interest in development of biobased sorbents for water treatment. Here in we reported, the fabrication of mechanically strong nanopapers by mixed dimensional assembly of 1D Cellulose nanofibers and 2D amino functionalized graphene oxide for water treatment. The fabricated amino functionalized GO/ cellulose nanofiber (AMGO-CNF) nanopaper showed superior antibacterial resistance towards *Escherichia coli* MTCC 1610 and *Klebsiella* due to the enhanced surface roughness which was confirmed from SEM and AFM studies. The amino group present in the AMGO enhanced the adsorption efficiency of the nanopaper towards methyl orange dye. The fabricated nanopaper showed an adsorption of 11.05 mg/gm 30 mg/L concentration at pH 2. Maximum adsorption was observed at pH 2 which was due to protonation of amine group. Moreover, the fabricated membrane showed excellent hydrolytic stability which can be corroborated to the surface roughness and reduced hydrophilicity. The investigation into the surface chemistries of cellulose nanofibers beyond the adoption of toxic solvents can enhance the economic usefulness of the process and yield a new eco-friendly adsorbent material that is agreeable to adsorbing various toxic pollutants.

✉ Deepu A. Gopakumar
deepu1789@gmail.com

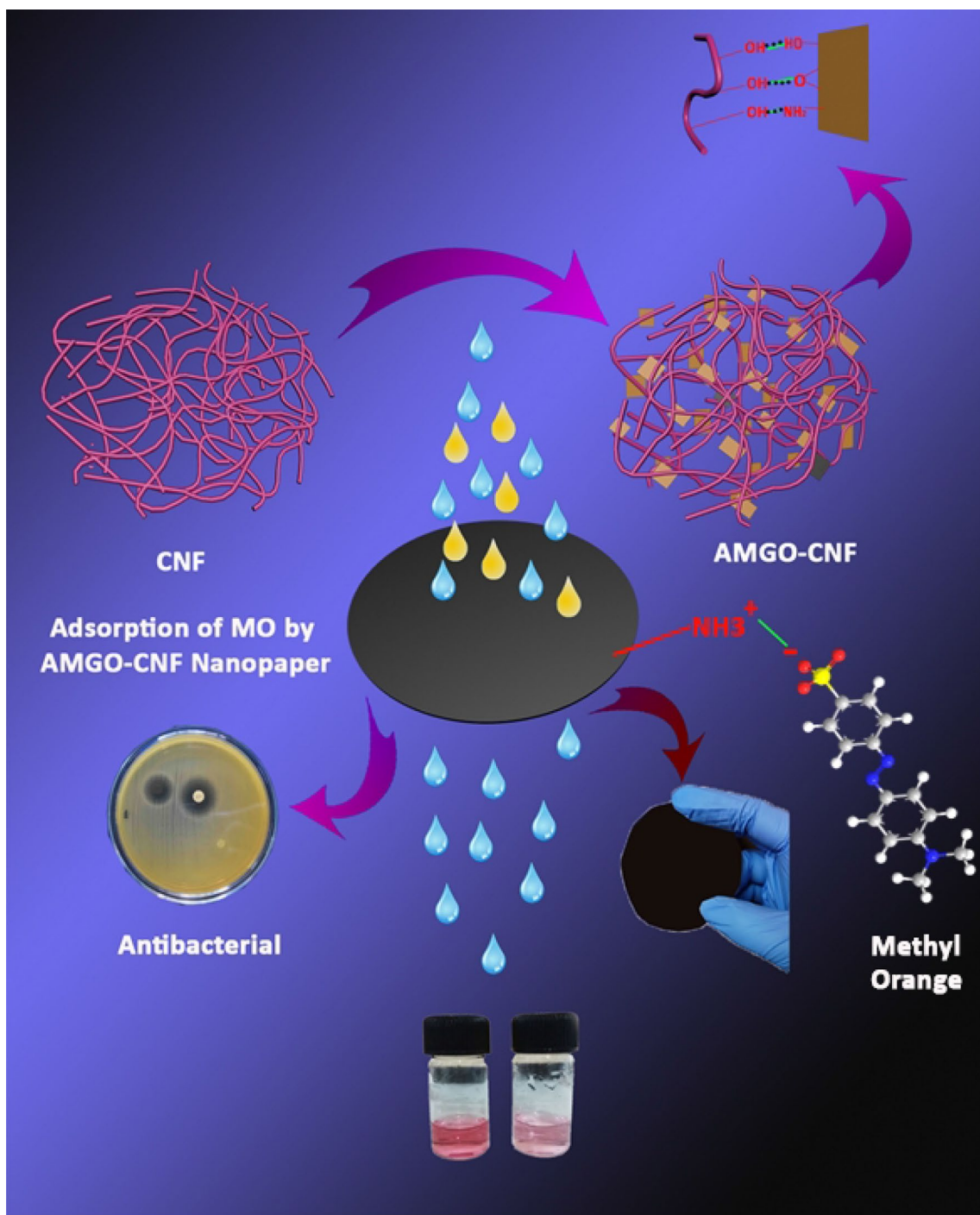
¹ School of Chemical sciences, Mahatma Gandhi University, Kottayam, Kerala 686560, India

² Department of Chemistry and Chemical engineering, Chalmers University of technology, Gothenburg, Sweden

³ School of Bio sciences, Mahatma Gandhi University, Kottayam, Kerala 686560, India

⁴ Chemistry Institute, Federal University of Uberlandia-UFU, Campus Santa Monica- Bloco1D-CP 593, Uberlandia, Brazil

⁵ Université de Toulouse, IMT Mines Albi, RAPSODEE CNRS UMR-5302, Campus Jarlard, Albi Cedex 09 81013, France



Keywords Cellulose nanofibers · Graphene oxide · Water purification

Introduction

The rising industrialization has polluted the fresh water resources to such an extent that the survival has become a

threat [1]. With the development of newer varieties of modern industries, the pollutants like toxic textile dyes, bacteria, suspended minute particles entering into fresh water resources are bound to go on enhancing [2]. Therefore the

removal of dyes, bacteria and suspended minute particles has become an integral discussion of our technological society. Another major effect due to industrial effluents is the rise in pathogenic bacteria [3]. These bacteria can be distinguished into two categories, gram negative and gram positive, gram negative being reported as most hospital-acquired infectious species [4]. *Escherichia coli* and *Klebsiella pneumoniae* are two gram-negative bacteria and their presence in water is ultimately pointing towards water pollution [5]. *E. coli* is considered as an indicator of the bacteriological quality of water [6].

Biological processes, chemical processes, operation of electromagnetic radiation etc. are the common removal techniques [7]. From these techniques ultrafiltration (UF), microfiltration (MF), and nanofiltration (NF) with pressure driven techniques have achieved substantial attention owing to their remarkably high performance and cost effective in nature [8]. Now a days, numerous scientists across the world have been extensively using electrospinning technology to fabricate water filtration membranes with high strength and uniform pore size [9]. However, the electrospinning technique is too costly to commercialize at industrial level. In this context an eco-friendly, cost effective and efficient method is very crucial since the commercially available synthetic polymer membranes eventually end up as non-degradable waste.

Biopolymers, due to its excellent biodegradability and physiochemical properties has gained immense attention and presumably replacing all the other commercial materials same time offering best prospects [10]. Among the numerous biopolymers, isolated cellulose stands foremost due to its excellent chemical, physical and biodegradable properties [11]. Cellulose are bio polymers mostly isolated from wood [12, 13]. Other sources include algae, bacteria and tunicate, the only animal resource [14]. The extracted cellulose nanofibers have inherent properties such as good mechanical properties and high specific surface area [15]. One dimensional (1 D) cellulose nanofibers (CNFs) are one of the promising adsorbent materials for water purification due to their low cost, abundant hydroxyl groups, natural abundance, and ecofriendly nature [16]. Additionally, the CNFs have the immense amount of surface hydroxyl (OH) groups, which facilitates diverse surface modifications via incorporation of chemical moieties that may lead to the adsorption toward the various pollutants in water [17]. On the other hand, Graphene oxide (GO) is another class of cost effective two dimensional (2D) nanomaterial emerged in recent years which could be effectively used for water purification [18]. The highly reactive nature of GO due to hydroxy, epoxy and carboxylic groups enables various surface chemistries which can be explored for the removal of various pollutants from water [19].

Until, there has been no studies reported on amino functionalized GO/cellulose nanofiber (AMGO-CNF) nanopaper

for water purification. The study carried out by Zhu et al. reported a cellulose-GO hybrid membrane for water purification [20]. The demonstrated membrane had a synergistic property of adsorption of Cu (II), flexibility, hydrolytic stability and mechanical robustness. Another work reported by Fryczkowska et al. investigated the physico-chemical and transport properties of GO/Cellulose membranes [21]. Meng et al. shredded light on toughening mechanism of cellulose nanopaper by developing a multiscale crack-bridging model [22]. Meng et al also developed a theoretical model to understand the effect of nano-fiber alignment in fracture toughness of CNF nanopaper [23]. A review by Meng et al. discusses the effect of orientation, polymerization degree, density, porosity and humidity of nanopaper, lignin on the mechanical properties of CNF nanopaper [24]. In this context, we are intended to fabricate a novel functional nanopaper by mixed dimensional assembly of 1D Cellulose nanofibers (CNFs) and 2D Amino functionalized graphene oxide (AMGO) via simple vacuum filtration process for removing toxic textile dyes. We have functionalized the GO to introduce amine groups on the surface of nanopaper in order to enhance the adsorption towards anionic dyes as well as introduce excellent antibacterial property.

Experimental Section

Materials

Cellulose nanofibers (CNFs) were procured from SUZANO, Brazil with diameter in the nano range of 20–30 nm. Graphene Oxide was synthesised in lab using Improved Hummers Method. Methyl Orange, sulphuric acid, phosphoric acid, KMnO_4 were purchased from Sigma Aldrich.

Synthesis of Graphene Oxide

Graphene oxide (GO) was prepared by modified hummers method using KMnO_4 as oxidising agent. 3:1 ratio of sulphuric acid and phosphoric acid were taken, onto which 0.09 gm of graphite powder were added under constant stirring. Oxidising agent KMnO_4 0.9 gm was added when uniform dispersion was achieved, and the mixture was stirred for 7 h. 15 ml of hydrogen peroxide was added to react any remaining reactant. The resultant GO was washed with ethanol and water till the pH was adjusted to 7 [25].

Amino Functionalization of Graphene oxide

A hydrothermal method was employed for functionalization of Graphene Oxide [26]. 0.5 gm of hydrous ferric chloride, 3 gm of Sodium acetate and functionalising agent Diethylene Triamine were stirred vigorously for 1 h on a magnetic

stirrer. The mixture was transferred to a stainless-steel enclosed Teflon autoclave and reacted at 200 °C for 6 h. After cooling to room temperature, the product was washed with ethanol and deionized water for several times to remove any unreacted product. The final product, amine functionalised Graphene oxide AMGO was dried at 60 °C for 24 h.

Fourier Transform Infrared Spectroscopy, Raman Spectroscopy and XRD Analysis

The prepared graphene oxide and amine functionalised graphene oxide were characterised using Fourier Transform infrared spectroscopy from 4000 to 400 cm^{-1} wavelengths to confirm the materials. FT-IR on fabricated nanopapers were also carried out. Raman imaging of graphene oxide and amine functionalised graphene oxide were recorded from 200 to 2000 cm^{-1} using Spectroscopy Model Alpha 300R. The X-ray diffraction (XRD) diffraction patterns were obtained at diffraction angles between 5° and 40° with a scanning rate of 0.4°/min at room temperature using Rigaku MiniFlex600 XRD analyser.

Scanning Electron Microscopy and Atomic Force Microscopy

The morphology of cellulose and AMGO-CNF nanopapers were examined using Scanning Electron Microscopy JEOL-Model JSM 6390. Samples were gold sputtered in an argon atmosphere. Analysis was carried out at 20 KV with 20 μm magnification. Surface roughness of nanopapers was analysed using Atomic Force Microscopy (A.P.E Research, Italy). The nanopapers were cut into 0.25 cm^2 size area and attached to plate of area 50 cm^2 using a double-sided tape. The nanopapers were characterized by a size of 2.5 \times 2.5 μm with an aid of tapping tool.

UV-Visible Spectrophotometer

Anionic dye adsorption was evaluated using Thermo Scientific Evolution 201 UV-Vis Spectrophotometer by absorbance technique. Samples were tested at different time intervals by pouring the solution to UV cuvette. Calibration of the sample for absorbance was done using water as reference. The absorbance was measured at 507 nm. Concentration of starting and final solutions were determined by UV-Vis spectroscopy.

Evaluation of Porosity of CNF and CNF-AMGO Nanopaper

The porosity of CNF and CNF-AMGO nanopaper were determined using gravimetric method using following Eq. (1),

$$\text{Porosity } \epsilon = (W_w - W_d) / A \times L \times \rho \quad (1)$$

where W_w and W_d is wet and dry weight of nanopaper respectively, A is the nanopaper effective area, L the thickness of the membrane and ρ is the density of water.

The average nanopaper pore radius was calculated by Guerout Elford-Ferry Equation given in Eq. (2)

$$\sqrt{(2.9 - 1.75\epsilon)8nLQ / \epsilon \times A \times \Delta P} \quad (2)$$

where n is the water viscosity [(8.9 $\times 10^{-4}$ Pa s) Q is water flux (m^3/s^{-1}) and ΔP operational pressure which is 1.5 bar pressure. The flux was calculated using dead end filtration technique using Sterlitech model HP4750 stirred cell shown in Fig. 1.

Evaluation of Anionic Dye Adsorption by AMGO-CNF Nanopaper

Methyl orange (MO) was used as a model compound for the anionic dye adsorption study. Various concentration of dyes was prepared for this study 5, 10, 20 and 30 mg/l respectively. Initially, 0.5 gm of AMGO-CNF nanopaper was weighed and immersed in 50 ml of dye solution, placed on a shaking bed at ambient temperature. At different time intervals the samples were collected to evaluate the concentration of dye. The study was carried out at varying pH of 2, 5, 7 and 10. The adsorption efficiency of the AMGO-CNF nanopaper was assessed from change in concentration of



Fig. 1 Dead end filtration technique using Sterlitech model HP4750 stirred cell

MO solution before and after the test using UV spectroscopy at 507 nm. Absorbance of the nanopaper was calculated using Beer Lambert's equation and adsorption capacity were evaluated by following equation [27].

$$\text{Adsorption Capacity (mg/g)} = (C_0 - C) L/G \quad (3)$$

where C_0 is initial concentration, C is the concentration at time T , L is volume of solution taken for test and G is weight of nanopaper (g).

Antibacterial Action of the Fabricated AMGO-CNF Nanopaper

Antibacterial studies were carried out on cellulose and modified nanopapers via Kirby Bauer Disc diffusion method[28]. A 4 mm thick Mueller–Hinton Agar plates were prepared after incubation for 20 min at 121 °C. Test organisms such as *E. Coli* MTCC 1610 and *Klebsiella*, (Gram Negative) were used in this study. Inoculum preparation was done using a log phase method where four to five well isolated colonies of bacteria were transferred from an agar plate using a loop to a Muller-Hinton broth. This was then incubated at 35 °C until a turbidity of 0.5 McFarland standard was achieved (approx. 1 to 2×10^8 CFU ml^{-1}). BaSO_4 turbid solution was used as a standard for inoculum density. This solution was equivalent to 0.5 McFarland standard. The bacterial suspension was uniformly inoculated to a prepared MHA plate using a sterilise swap. The cellulose and AMGO-CNF nanopaper were placed on to this agar plate using a sterilise forceps. These discs were gently pressed to get complete contact with the agar surface. Streptomycin (25 μg per disc) were used

as positive control for all the bacteria. These plates were incubated at 37 °C for 20 h. After 20 h zone of inhibition was measured.

Contact Angle of Fabricated AMGO-CNF Nanopaper

In order to determine the extent of hydrophilicity, the contact angle test was carried out using SEO-Phoenix 300 model. The source light was focused on instrument on hand camera and deionized water was used as probe liquid. Three contact angles were measured at different places of the sample and the average value is reported.

Mechanical Property of AMGO-CNF Nanopaper

Mechanical test was conducted using UTM model Tinius Olsen H50KT. Samples were prepared with a thickness of 5 mm and the test was conducted with a deformation of 5 mm min^{-1} using 100 N load cell.

Result and Discussion

Characterisation of GO and AMGO Using FT-IR and Raman Spectroscopy

In order to confirm the amine functionalization on GO, FTIR and Raman spectroscopy of both graphene oxide (GO) and amino functionalized graphene oxide (AMGO) were studied [26]. Figure 2a shows the FTIR and Raman spectra of GO and AMGO. From the Fig. 2, GO shows peak at 1041 cm^{-1} (C–O epoxy stretching), 1220 cm^{-1} (C–OH stretching), 1625

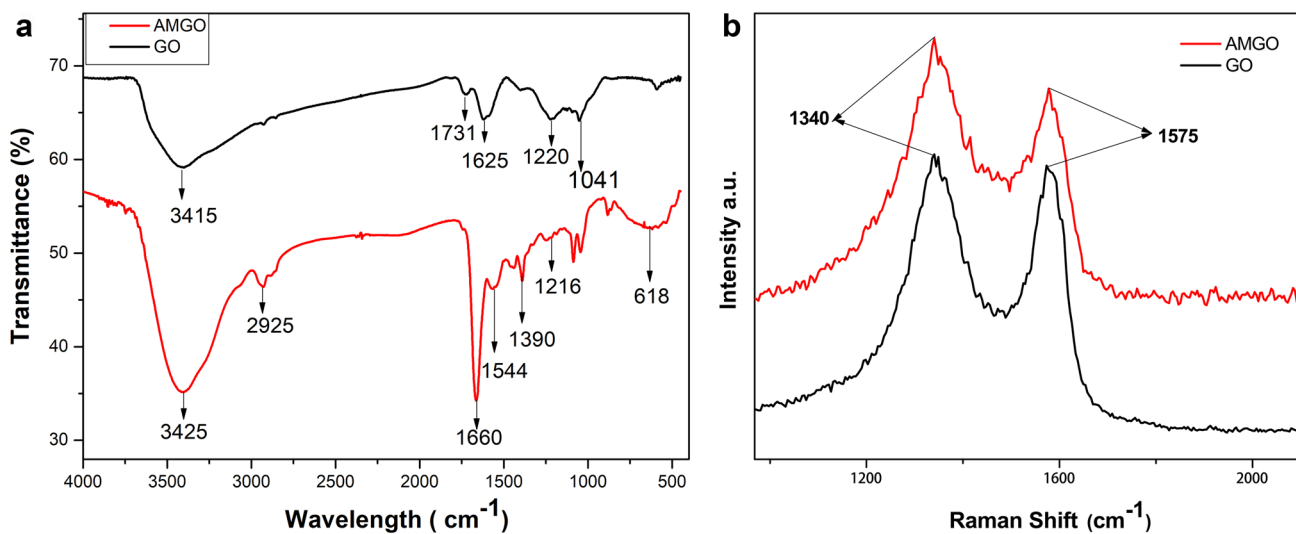


Fig. 2 a FTIR Spectrum of GO and AMGO and b Raman spectra of GO and AMGO

cm^{-1} (C=C stretching), 1731 cm^{-1} (C=O stretching) and 3415 cm^{-1} (–OH stretching). The presence of these groups confirmed the formation of GO. In the case of AMGO, a new peak has emerged at 1390 cm^{-1} indicating the C–N stretching vibration. The band at 1544 cm^{-1} was attributed to the formation of stretching and bending vibration of N–H Bond. Medium peaks or bands at free region can be described as asymmetric C–N vibration coupled with NH_2 or N–H modes. The disappearance of peak at 1731 cm^{-1} (C=O stretch of COOH) of FTIR spectrum in AMGO confirms the successful amino functionalization of GO[29]. Raman spectroscopy showed the presence of defects on graphite layer. Figure 2b shows the Raman spectra of GO and AMGO. Figure 2b shows two peaks at 1340 cm^{-1} and 1575 cm^{-1} for both GO and AMGO which can be attributed to D band and G band respectively. D band represents the defect band (SP^3 carbon) and G band contributes to graphitic structure (SP^2 carbon in Graphite sheet). The ratio of D and G band gives the defect ratio. Compared with GO, the defect ratio of AMGO was increased which confirmed the successful amine functionalization on GO [30].

Fabrication of AMGO-CNF Nanopaper

Nanopapers were prepared using vacuum filtration technique [31]. 20 gm of cellulose (3 wt%) and 10% AMGO (w.r.t cellulose wt%) were mixed and dispersed using a homogenizer (IKA-25 ULTRA TURRAX). When proper homogeneous dispersion was achieved, the dispersion was casted into nanopaper using vacuum filtration. The fabricated nanopapers were peeled off from the filter and dried on a hot press for 30 min at $60 \text{ }^\circ\text{C}$. Figure 3 shows the fabrication of AMGO-CNF nanopaper via vacuum filtration and possible interaction of cellulose and AMGO. The AMGO nanosheets effectively interact with cellulose nanofibers through strong hydrogen bonding interactions as shown in Fig. 3.

FTIR and XRD Studies of CNF and AMGO-CNF Nanopaper

CNF and AMGO-CNF nanopaper were characterised using ATR-FTIR [32]. Figure 4a shows the FTIR spectra of CNF and AMGO-CNF nanopaper. The peaks of CNF nanopaper show a typical saccharide structure. The peaks at 3335

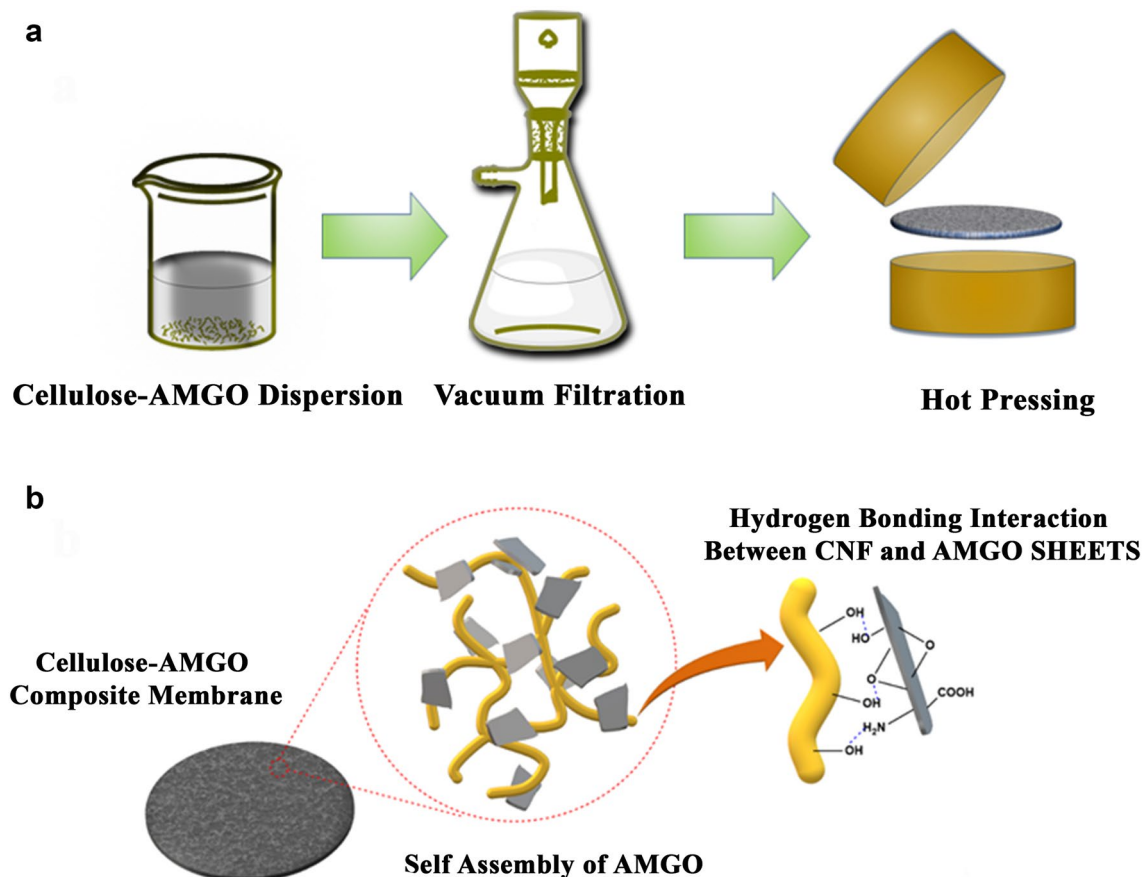


Fig. 3 a Strategy for the Fabrication of AMGO-CNF nanopaper b possible interaction between AMGO and cellulose nanofibers (CNF)

cm^{-1} ($-\text{OH}$ vibration), 2910 cm^{-1} ($\text{C}-\text{H}$ stretching), 1362 cm^{-1} ($-\text{CH}_3$ vibration), 1159 cm^{-1} ($\text{C}-\text{O}-\text{C}$ anti-symmetric stretching), 1030 cm^{-1} ($\text{C}-\text{C}-\text{O}$ stretching), 890 cm^{-1} ($\text{C}-\text{C}$ stretching), confirmed the cellulosic structure of nanopaper. In the case of AMGO-CNF nanopaper, two distinct sharp peaks at 3330 cm^{-1} and 3280 cm^{-1} attributed to NH stretch, which overlapped with the broad peak arisen from carboxylic acid stretch. Also, compared to CNF the band width at 3330 cm^{-1} and intensity of all peaks attributed to OH functional group decreases remarkably which indicates effective reduction of oxygen species during the amination process.

Figure 4b shows the XRD spectrum of AMGO, CNF and AMGO-CNF nanopaper. It was clearly evident that, the XRD spectrum of CNF nanopaper showed peaks at $2\theta = 16.3^\circ$ and 22.6° corresponding to (110) and (200) planes. These are typically attributed to cellulose type I structure. AMGO displayed a broad peak at $2\theta = 25.9^\circ$ corresponding to the (002) plane of graphitic phase, indicating high extent of reduction [33]. The incorporation of AMGO into CNF matrix affects the crystallinity of CNF. At lower concentration AMGO loading, the AMGO aligned in parallel and facilitated an ordered alignment of CNF molecules leading to an increased crystallinity. These findings were well agreement with Phiri et al. where they showed the enhancement of crystallinity of micro fibrillated cellulose (MFC) upon the incorporation of reduced graphene oxide (RGO) [34]. The enhancement in crystallinity could influence the mechanical properties and porosity.

Morphology and Porosity of Fabricated CNF and AMGO-CNF Nanopaper

Figure 5 shows SEM images of CNF and AMGO-CNF nanopaper [20]. SEM image of CNF displays a nonporous nanofiber arrangement. They are randomly arranged and have empty spaces between fibres. With the addition of AMGO, the empty spaces were filled, and a compact structure could be seen from the SEM image. 3D topological image of CNF and AMGO-CNF nanopaper were shown in Fig. 5b. Surface roughness value mainly depends on three factors, root mean square (R_q), arithmetic mean deviation of roughness (R_a), and height difference between five maximum height peak (R_{max}) and five minimum height peaks (R_{min}). Usually R_a is considered to scrutinize the roughness nature. From Table 1 the cellulose nanopaper showed a R_a value of 7.34, without any addition of AMGO. Further, with addition of AMGO, AMGO-CNF nanopaper showed a R_a value of 15.50. The addition of AMGO resulted in the enhanced surface roughness to a greater value. This higher value of R_a might be due to the uniform dispersion of AMGO nanoparticles on the surface

The porosity of CNF and CNF-AMGO nanopaper were determined using gravimetric method using Eq. (1) and the average nanopaper pore radius was calculated by Guerout Elford-Ferry equation given in Eq. (2) in the experimental section [35]. The porosity percentage was found to be 32% and 51% for AMGO-CNF and CNF nanopaper respectively whereas the average pore radius was found to be 1.9 nm and 3.2 nm for AMGO-CNF and CNF nanopaper respectively.

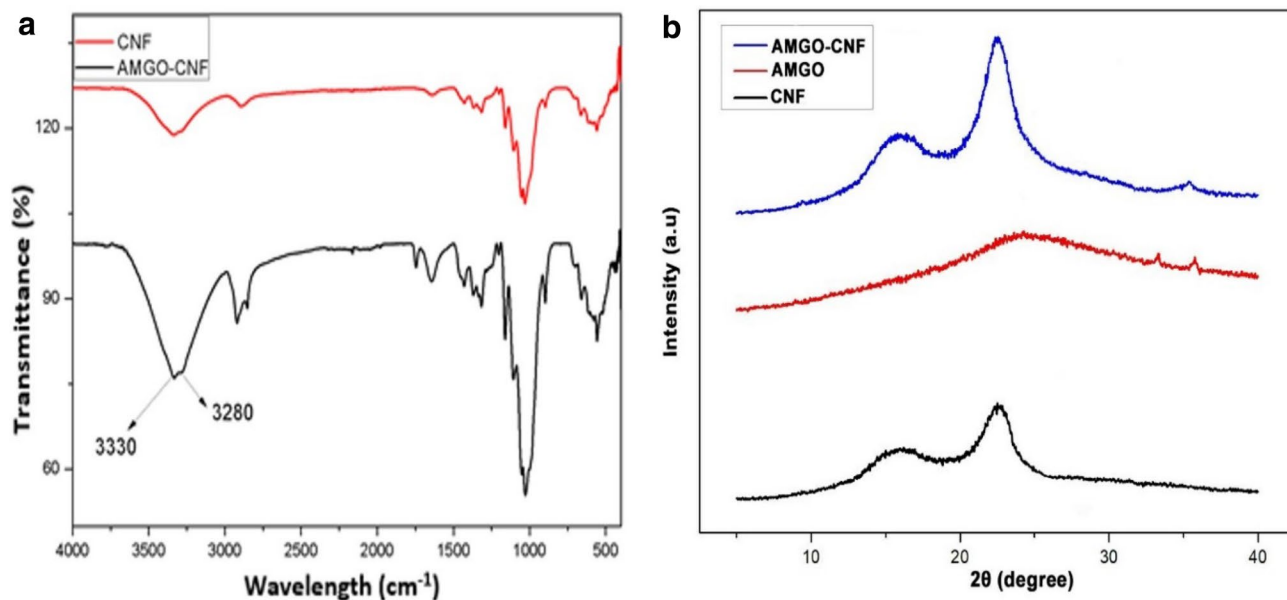


Fig. 4 a FT-IR Spectrum of CNF and AMGO-CNF nanopaper and b XRD spectrum of AMGO, CNF and AMGO-CNF nanopaper

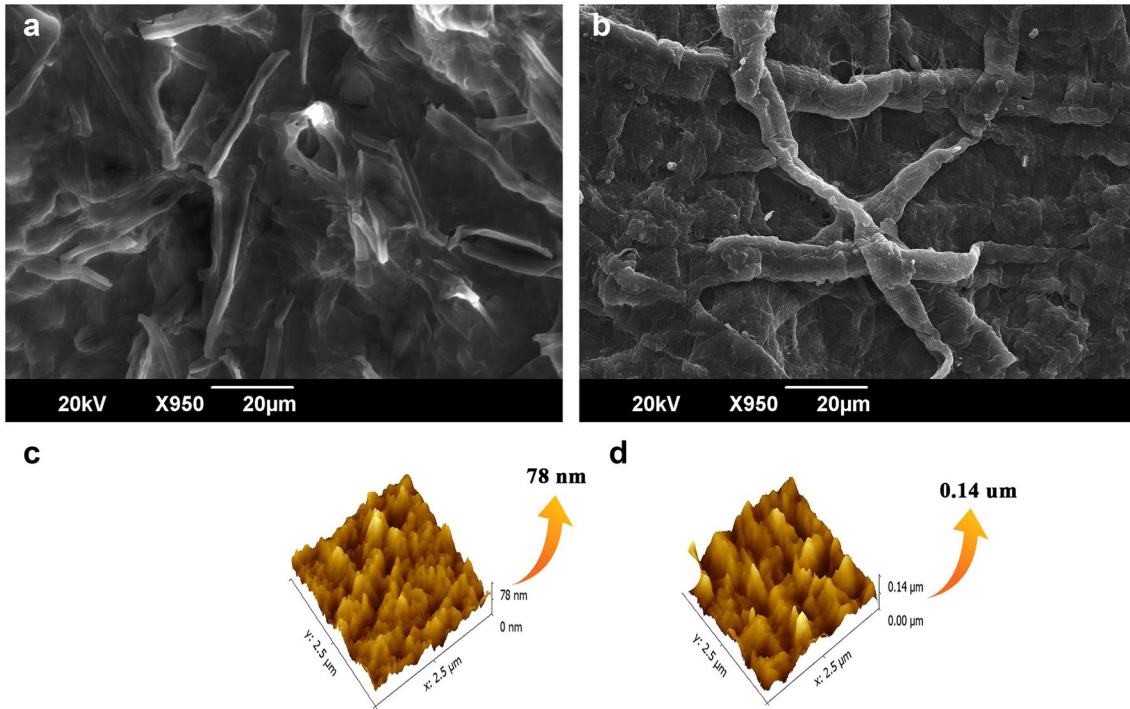


Fig. 5 SEM and AFM images of CNF and AMGO-CNF nanopaper

Table 1 Surface roughness of nanopapers

Nanopaper	Ra	Rq	Rz	Rmax
CNF	7.34	9.51	0.00	78.21
AMGO-CNF	15.5	19.70	0.00	141.40

Evaluation of Adsorption Capacity of AMGO-CNF Nanopaper Against Anionic Methyl Orange Dye

UV spectroscopy was employed to determine the adsorption capacity of AMGO-CNF nanopaper against anionic dye [36]. Here, we used methyl orange as a model for negatively charged dye. Figure 6 illustrates the adsorption capacity of AMGO-CNF nanopaper as a function of time with different pH conditions. Result shows that, maximum adsorption was observed at pH 2 with an adsorption value of 7.62 mg/g at 20 mg/L concentration. Figure 7 illustrates the proposed removal mechanism of methyl orange (MO) dye by AMGO-CNF nanopaper. Amine groups in AMGO either could be protonated at lower pH to form NH_3^+ ($\text{R-NH}_2 + \text{H}^+ \rightarrow \text{NH}_3^+$) or deprotonated at lower pH to form $\text{NH}_2 \dots \text{OH}^-$. Zeta potential of different pH were carried out and found the value of pH_{zpc} (Zero Point Charge Fig) of 5.9. pH below the pH_{zpc} , AMGO had positive charge and anionic dyes were adsorbed on to the surface of AMGO-CNF nanopaper by electrostatic interaction. The negatively charged anionic dyes were easily

adsorbed by positively charged surface of AMGO in the fabricated nanopaper. At higher pH, the demonstrated AMGO-CNF nanopaper showed a decreased adsorption capacity which might be due to the decrease in extend of protonation.

Adsorption Isotherm and Adsorption Kinetics

Adsorption isotherm describes the equilibrium relationship between adsorbent and adsorbate [37]. This equilibrium data which describes the interaction of dyes with adsorbent can be expressed via a series of models. Some of the commonly investigating models are Langmuir and Freundlich [38].

$$\text{Langmuir Equation: } Q_e = Q_0 K_{\text{lang}} C_e / (1 + K_{\text{lang}} C_e) \quad (4)$$

$$\text{Linear Form } C_e/Q_e = 1/Q_0 K_{\text{lang}} + C_e/Q_0 \quad (5)$$

where C_e , Q_e , Q_0 and K_{lang} are equilibrium concentration of dye solution (mg/L), amount of dye adsorbed by nanopaper (mg/g), maximum adsorption capacity of nanopaper (mg/g) and Langmuir constant.

$$\text{Freundlich Equation : } \log Q_e = \log K_f + (1/n) \log C_e \quad (6)$$

K_f is the Freundlich constant and n the heterogeneity factor. n describes absorbent's adsorption intensity.

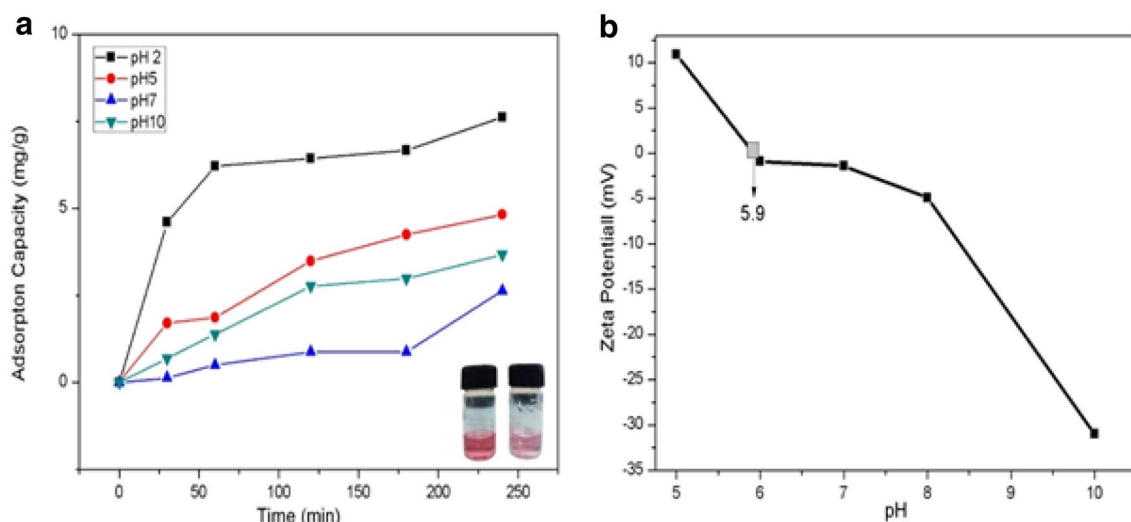
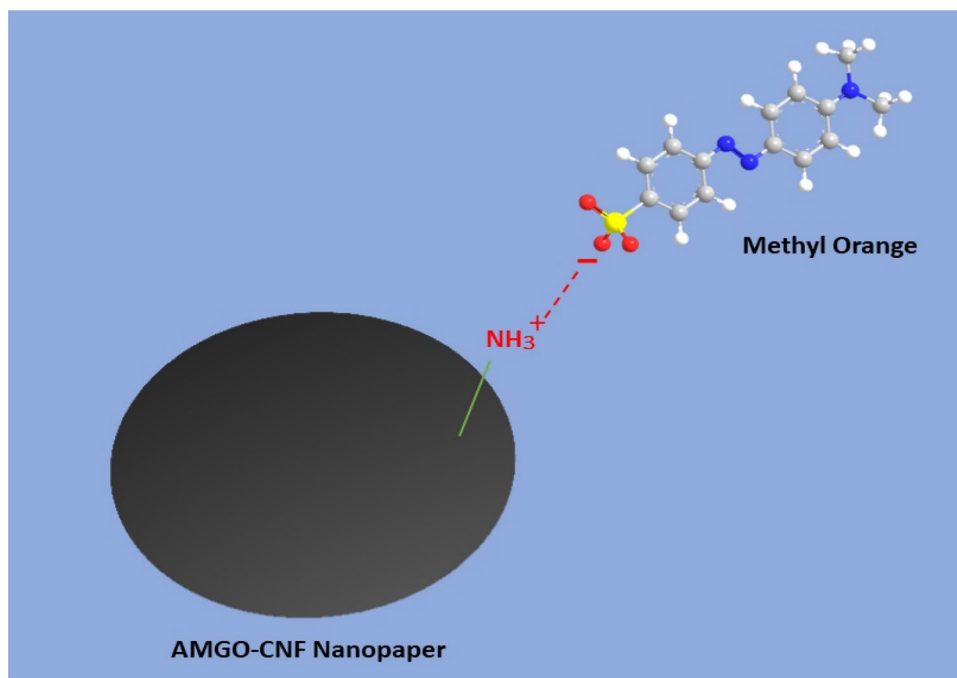


Fig. 6 Adsorption capacity AMGO-CNF nanopaper with **a** varying pH and **b** zeta potential

Fig. 7 Proposed removal mechanism of MO dye by fabricated AMGO-CNF nanopaper



Adsorption isotherm data were plotted using above equations. Other parameters were calculated from linear regression plotting. Langmuir and Freundlich models were plotted out of which Freundlich model apparently fitted better. Figure 8a shows, the Freundlich model fitting with a correlation coefficient of $R^2=0.919$ and shows that, the adsorption of methyl orange to AMGO-nanopaper via multilayer adsorption. Freundlich theory is based on parameter of $1/n$ value. Here we got $1/n$ value of 1.44 which indicates the adsorption was S-type isotherm. This type of isotherm has been

observed in low concentration ranges with a polar functional group [39].

Adsorption kinetics explains the rate of chemical reaction and factors affecting the reaction rate [37] Pseudo first order kinetic model and pseudo second order kinetic model were used for kinetic studies.

A linear form of both equations are as follows:

$$\text{Pseudo First order : } \log (Q_e - Q_t) = \log Q_e - K_1 t / 2.303 \quad (7)$$

$$\text{Pseudo Second order} : t/Q_t = 2/K_e Q_e^2 + (1/Q_e) t \quad (8)$$

Rate constants and equilibrium adsorption capacity were tested for Pseudo-First order (PFO) and Pseudo-Second order (PSO). Methyl orange adsorption did not follow the pseudo first order (correlation coefficient less). Moreover, pseudo second order showed good correlation for the experiment data (Fig. 7b). Plots of t/q_t and t showed good linearity. The PSO rate constant K_2 , calculated adsorption and the linear regression correlation coefficients value R^2 are given in Table 2. The calculated Q_e values were in well agreement with experimental adsorption value and correlation coefficient value R^2 are higher and close to one.

Antibacterial Action of Nanopapers

Biofouling due to the action of microbes such as bacteria and viruses is a major challenge for designing materials for water purification. Figure 9 shows the digital image of antibacterial action of AMGO-CNF and CNF nanopapers. The fabricated AMGO-CNF nanopaper showed superior antibacterial activity against *E. Coli* MTCC 1610 and *Klebsiellar*. The contact active antibacterial action of the AMGO-CNF nanopaper can be attributed to a combined effect of roughness and surface amino groups of AMGO in AMGO-CNF nanopaper. The characteristic outer membranes of gram-negative bacteria are responsible for their resistance towards antibiotics. The lipopolysaccharides in outer membrane contains phosphate group which would susceptible to interact with amino groups which resulted in the rupture of the bacterial membrane. Table 3 illustrates the zone of inhibition data for different bacteria.

Hydrophilicity of the Fabricated AMGO-CNF Nanopaper

Figure 10 shows the contact angle of CNF and AMGO-CNF nanopaper. Contact angle of CNF and AMGO-CNF nanopaper were found to be 43° and 71° respectively. The enhancement in contact angle of AMGO-CNF nanopaper was due to the decrease in the hydrophilicity of nanopaper. The OH groups of CNF could be interacted with amine groups of AMGO in AMGO-CNF nanopaper which resulted in the reduction of OH groups. This reduction in OH groups makes the nanopaper less hydrophilic compared with CNF nanopaper. Furthermore, surface roughness also could enhance the contact angle of AMGO-CNF nanopaper which was confirmed from the AFM studies.

Hydrolytic Stability of CNF-AMGO Nanopaper

Since the fabricated CNF-AMGO nanopaper are intended to use in water purification, it is very relevant to study the hydrolytic stability of these fabricated nanopapers. To investigate the water stability and reusability, the nanopaper were kept in water for 60 h. The pristine CNF nanopaper lost its

Table 2 Kinetic parameter for pseudo second Order

Concentration	q_e , cal (mg g^{-1})	K_2 ($\text{g mg}^{-1} \text{min}^{-1}$)	R^2
5 mg	1.19731	0.05169	0.98602
10 mg	2.3980	0.02554	0.9838
20 mg	7.5318	0.01087	0.96103
30 mg	11.0485	0.002879	0.9366

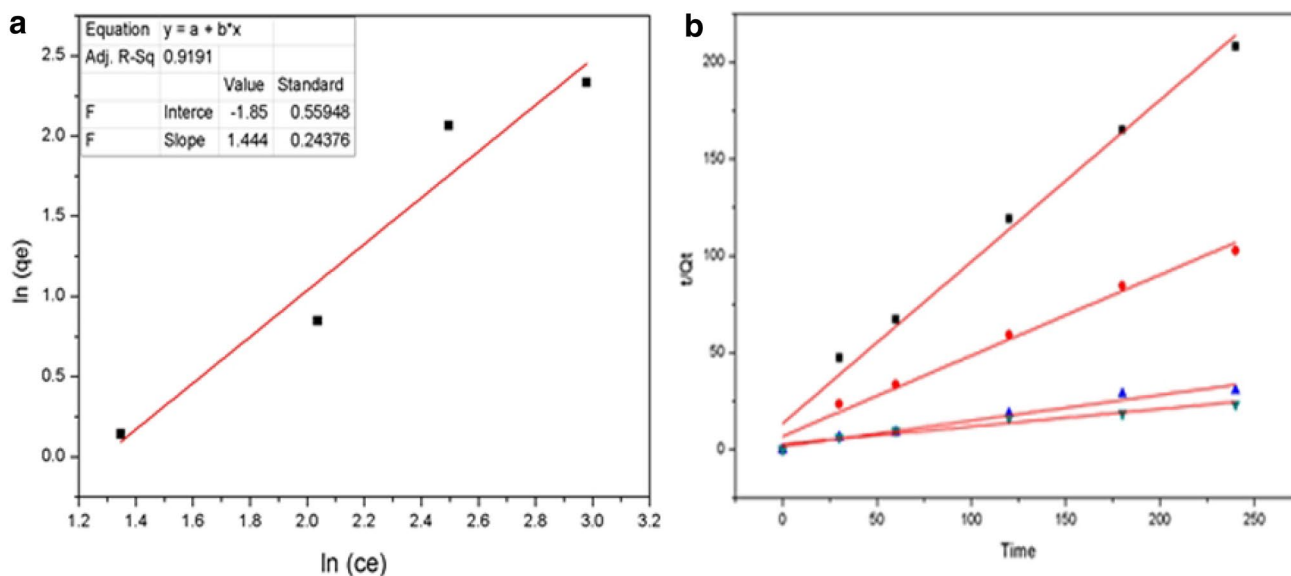


Fig. 8 **a** Freundlich model plot and **b** pseudo second order plot for experiment data

Fig. 9 Digital image illustrating the antibacterial activity of CNF and AMGO-CNF nanopaper

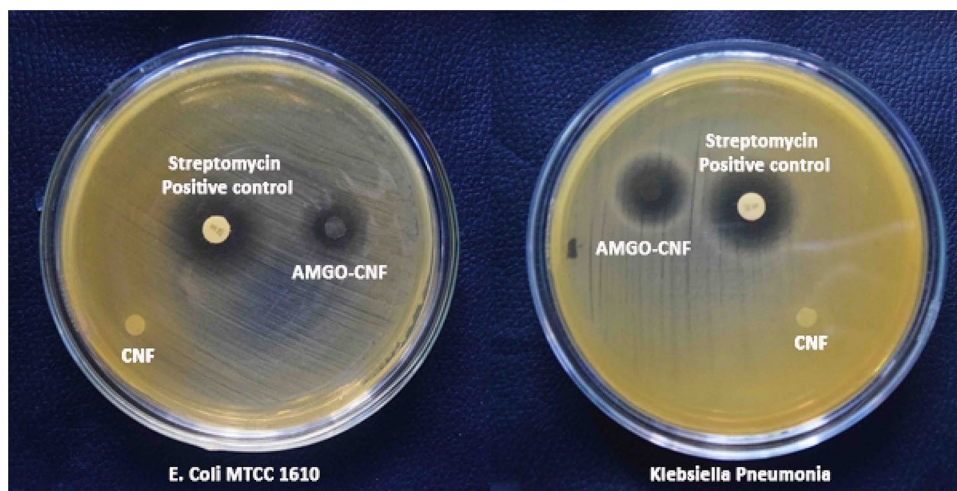


Table 3 Inhibition zone of fabricated AMGO-CNF nanopaper

Bacterium	Diameter (mm)	Zone of inhibition (mm)
<i>Escherichia Coli</i>	11	14
<i>Klebsiella pneumonia</i>	11	15

stability in water and structurally degraded after 60 h. Figure 11a shows and AMGO-CNF nanopaper before and after soaking in water. There was a weight loss of 28% in case of CNF nanopaper, whereas in AMGO-CNF nanopaper had a weight loss of 2%. In order to further investigate the hydrolytic stability, both nanopapers were subjected to sonication in water. Figure 11b illustrates the hydrolytic stability of both CNF and AMGO-CNF nanopapers after sonication in water for 30 min. The CNF nanopaper started to collapse within 1 min and completely dispersed in water within 4 min, whereas AMGO-CNF nanopaper had good hydrolytic stability even after the probe sonication for 30 min. The mechanical stability of the nanopaper depends on the structural integrity of the fibre network. The pristine cellulose nanopaper is hydrophilic compared to the fabricated AMGO CNF nanopaper which would undergo rapid swelling and became mechanically poor whereas decreased hydrophilicity in fabricated AMGO-CNF nanopaper reduced the interaction with the water molecules and there by enhanced the wet strength.

Wet Strength of the CNF-AMGO Nanopaper

Mechanical properties are crucial for nanopaper to work under stress [40]. The nanopapers those works under the pressure driven technology should have sufficient strength for their optimum performance. Table 4 shows the tensile

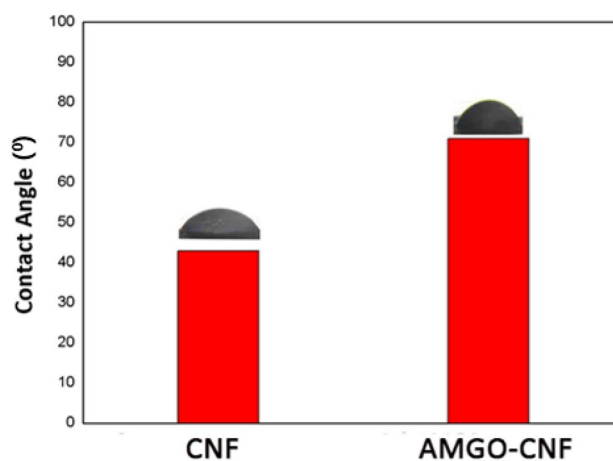


Fig. 10 Contact angle of CNF and AMGO-CNF nanopaper

strength of CNF and AMGO-CNF nanopaper under normal condition and under wet condition. Figure 12 depicts the stress by strain graph of wet CNF and wet AMGO-CNF nanopaper. Pristine CNF nanopaper had a tensile strength of 49.3 Mpa whereas AMGO-CNF nanopapers tensile strength reduces to 38.1 Mpa. Both fabricated nanopapers were immersed in water for 30 min in order to evaluate the wet strength. It was found that, pristine CNF nanopaper had a wet strength of 17.5 MPa, whereas AMGO-CNF nanopaper had wet strength of 25.9 MPa. The enhanced wet strength of AMGO-CNF nanopaper was due to the reduction of hydrophilicity after the incorporation of AMGO. The inherent hydrophilic nature of pristine CNF nanopaper resulted in the swelling of the cellulose nanofibers when comes in contact with water. Additionally, CNF nanopaper had 80% of increase in weight after soaking in water for half hour, whereas AMGO-CNF nanopaper only showed 30% increase

Fig. 11 Hydrolytic stability of CNF and AMGO-CNF nanopaper

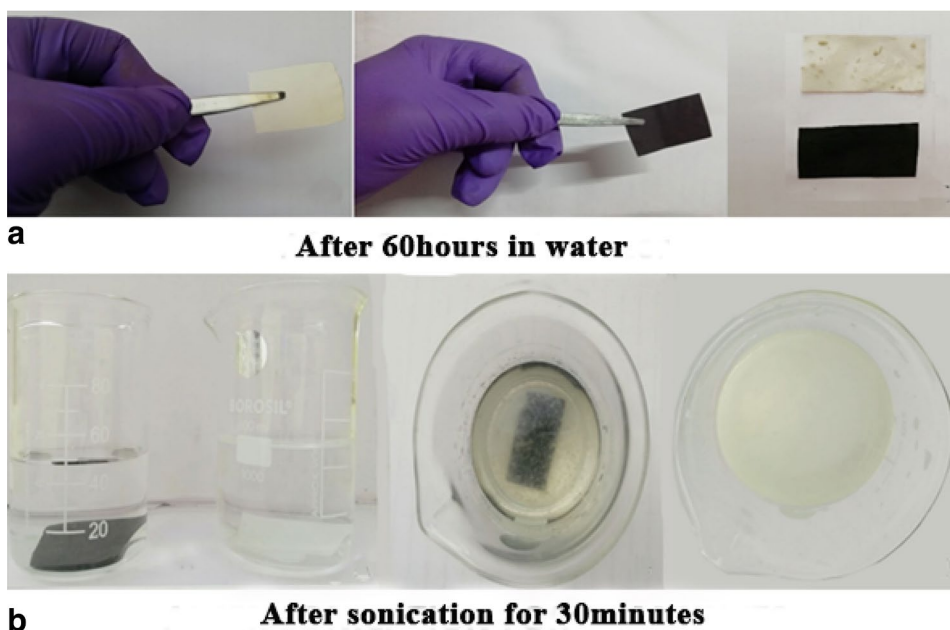


Table 4 Mechanical strength of CNF and AMGO-CNF Nanopapers

Specimen	Dry sample (Mpa)	Wet sample (Mpa)
CNF nanopaper	38.1	17.48
AMGO-CNF nanopaper	49.3	25.9

in weight. Amine functionalised graphene oxide (AMGO) being a strong material could interact with cellulose nanofibers which resulted in the decreased active sites for hydrogen bonding and thereby reduced the swelling behaviour.

Reusability of the AMGO-CNF Nanopaper

Figure 13 illustrates the reusability of CNF-AMGO nanopaper with 10% concentration[38]. The reusability of the nanopaper were investigated using 99% ethanol as desorption agent. These nanopapers were washed and dried at 50 °C for 12 h. It was found that, around 74% of adsorption retention was achieved after four times of reuse.

Conclusion

Herein we have fabricated a hybrid cellulosic and amine functionalized graphene oxide nanopaper via a simple vacuum filtration technique. Graphene oxide was prepared using modified hummers method and successfully amine functionalised under a controlled hydrothermal condition.

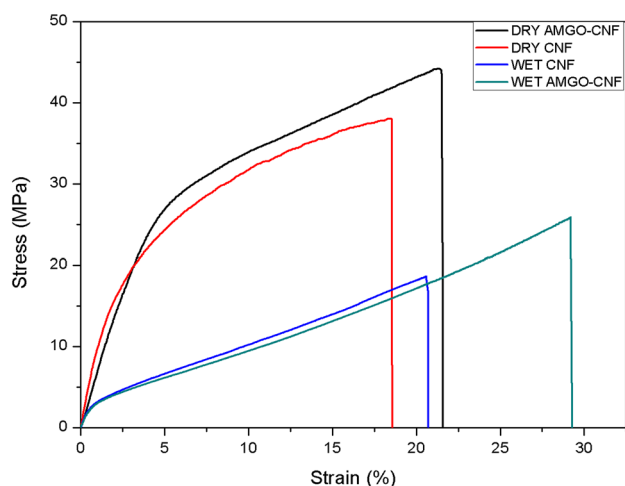


Fig. 12 Stress v/s strain graph of normal and wet nanopapers

This was confirmed by FT-IR and Raman Spectroscopy. The addition of AMGO on to cellulose nanofiber resulted in the enhanced surface roughness which was evident from SEM and AFM images. The increased surface roughness aids the anti-bacterial action of the nanopaper against *E. Coli MTCC 1610* and *Klebsiella*. The demonstrated AMGO-CNF nanopaper exhibited excellent antibacterial action and good anionic dye adsorption without compromising the strength factor. At 30 mg/l of MO dye, the fabricated AMGO-CNF paper showed an excellent adsorption of 11.05 mg/g at pH 2. This adsorption was due to the protonation of amine group. Moreover, it was found that, the protonation decreased with increase in pH. The adsorption data were plotted for adsorption isotherm and

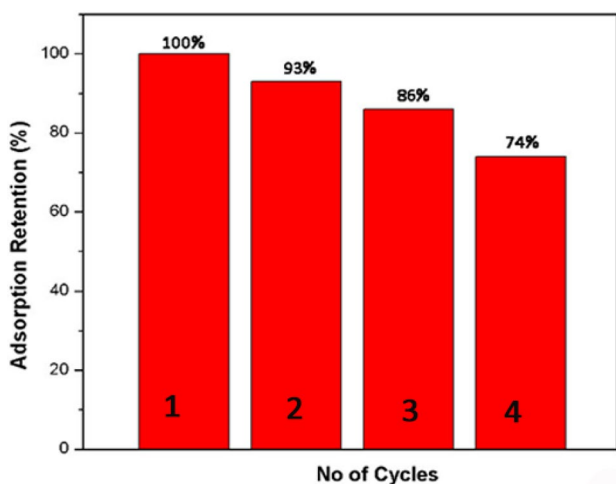


Fig. 13 Reusability of nanopaper after four times of adsorption

its kinetics were investigated. Additionally, the fabricated AMGO-CNF nanopaper exhibited good wet strength of 25.9 with excellent hydrolytic stability even after sonication for 30 min. Moreover, simple fabrication technique with enhanced antibacterial action and adsorption capability using less amount of AMGO opens new platform for the dye adsorption.

References

- Pathan TS, Thete PB, Shinde SE, Sonawane DL, Khillare YK (2009) *J Bot Res Int* 21:71–78
- Ebenstein A (2012) *Rev Econ Stat* 94:186–201
- Haq I, Raj A (2018) *Emerging eco-friendly approaches for waste management*. Springer, Singapore, pp 121–142
- Pfaller MA, Flamm RK, Mendes RE, Streit JM, Smart JI, Hamed KA, Duncan LR, Sader HS (2018) *Antimicrob Agents Chemother* 63:1–12
- Koksal E, Tulek N, Sonmez MC, Temocin F, Bulut C, Hatipoglu C, Erdinc FS, Ertem G (2019) *Invest Clin Urol* 60:46–53
- Odonkor ST, Ampofo JK (2013) *Microbiol Res (Pavia)* 4:2
- Yadollahpour A, Rashidi S, Ghotbeddin Z, Jalilifar M, Rezaee Z (2014) *J Pure Appl Microbiol* 8:3711–3719
- Castaing JB, Massé A, Pontié M, Séchet V, Haure J, Jaouen P (2010) *Desalination* 253:71–77
- Liang Y, Kim S, Kallem P, Choi H (2019) *Chemosphere* 221:479–485
- Andreeßen B, Lange AB, Robenek H, Steinbüchel A (2010) *Appl Environ Microbiol* 76:622–626
- Brinchi L, Cotana F, Fortunati E, Kenny JM (2013) *Carbohydr Polym* 94:154–169
- Zhao J, Zhang W, Zhang X, Zhang X, Lu C, Deng Y (2013) *Carbohydr Polym* 97:695–702
- Valencia L, Arumugan V, Jalvo B, Maria HJ, Thomas S, Mathew AP (2019) *ACS Omega* 4:4330–4338
- Zhao Y, Moser C, Lindstrom ME, Henriksson G, Li J (2017) *ACS Appl Mater Interfaces* 9:13508–13519
- Espino-Pérez E, Bras J, Ducruet V, Guinault A, Dufresne A, Domenek S (2013) *Eur Polym J* 49:3144–3154
- Nechyporchuk O, Belgacem MN, Bras J (2016) *Ind Crop Prod* 93:2–25
- Xu X, Zhao G, Wang H, Li X, Feng X, Cheng B, Shi L, Kang W, Zhuang X, Yin Y (2019) *J Power Sources* 409:123–131
- Compton OC, Nguyen ST (2010) *Small* 22:711–723
- Kim F, Cote LJ, Huang J (2010) *Adv Mater* 22:1954–1958
- Zhu C, Liu P, Mathew AP (2017) *ACS Appl Mater Interfaces* 9(24):21048–21058
- Fryczkowska B, Wiechniak K (2017) *Polish J Chem Technol* 19:41–49
- Meng et al (2017) *J Mech Phys Solids* 103:22–39
- Meng et al (2018) *Eng Fract Mech* 194:350–361
- Meng, Wang (2019) *Appl Mech Rev* 71(4):040801
- Marcano DC, Kosynkin DV, Berlin JM, Sinitskii A, Sun Z, Slesarev A, Alemany LB, Lu W, Tour JM (2010) *ACS Nano* 4(8):4806–4814
- Zhao D, Gao X, Wu C, Xie R, Feng S, Chen C (2016) *Appl Surf Sci* 384:1–9
- Annadurai G, Juang RS, Lee DJ (2002) *J Hazard Mater* 92:263–274
- Elias E, Chandran S, Zachariah AK, Vineesh Kumar VK, Sunil MA, Bose S, Souza FG, Thomas S (2016) *RSC Adv* 6:85107–85116
- Shanmugaraj AM, Yoon JH, Yang WJ, Ryu SH (2013) *J Colloid Interface Sci* 401:148–154
- Zhang W, Ma J, Gao D, Zhou Y, Li C (2016) *Prog Org Coat* 94:9–17
- Gopakumar DA, Pai AR, Pottathara YB, Pasquini D, Carlos L, De Morais M, Luke N, Kalarikkal Y, Grohens, Thomas S (2018) *ACS Appl Mater Interfaces* 10:20032–20043
- Garside P, Wyeth P (2006) *Stud Conserv* 51:205–211
- Mahdavi H, Kahriz PK, Rajbar HG, Shahalizade T (2017) *J Mater Sci Mater Electron* 28:4295–4305
- Phiri J, Johansson LS, Gane P, Maloney TC (2018) *Nanoscale* 10:9569–9582
- Guo J, Kim J (2017) *RSC Adv* 7:33822–33828
- Gopakumar DA, Pasquini D, Henrique MA, De Morais LC, Grohens Y, Thomas S (2017) *ACS Sustain Chem Eng* 5:22026–22033
- Chakraborty S, Chowdhury S, Das Saha P (2011) *Carbohydr Polym* 86:1533–1541
- Zhou Y, Zhang M, Hu X, Wang X, Niu J, Ma T (2013) *J Chem Eng Data* 58:413–421
- Limousin G, Gaudet JP, Charlet L, Szenknect S, Barthès V, Krimissa M (2007) *Appl Geochem* 22:249–275
- Wu YB, Yu SH, Mi FL, Wu CW, Shyu SS, Peng CK, Chao AC (2004) *Carbohydr Polym* 57:435–440